

Spokes cluster: The search for the quiescent gas [★]

Jaime E. Pineda^{1,2} and Paula S. Teixeira^{3,4}

¹ European Southern Observatory (ESO), Garching, Germany

² UK ARC Node, Jodrell Bank Centre for Astrophysics, School of Physics and Astronomy, University of Manchester, Manchester, M13 9PL, UK

e-mail: jaime.pineda@manchester.ac.uk

³ Universität Wien, Institut für Astrophysik, Türkenschanzstrasse 17, 1180 Vienna, Austria

e-mail: paula.teixeira@univie.ac.at

⁴ Laboratório Associado Instituto D. Luiz-SIM, Universidade de Lisboa, Campo Grande, 1749-016, Lisboa, Portugal.

Received ; accepted October 16, 2018

ABSTRACT

Context. Understanding the role of turbulent and thermal fragmentation is one of the most important current questions of star formation. To better understand the process of star and cluster formation, we need to study in detail the physical structure and properties of the parental molecular cloud. In particular, it is important to understand the fragmentation process itself; this may be regulated by thermal pressure, magnetic fields, and/or turbulence. The targeted region, the Spokes cluster, or NGC 2264 D, is a rich protostellar cluster where previous N_2H^+ (1–0) observations of its dense cores presented linewidths consistent with supersonic turbulence. However, the fragmentation of the most massive of these cores appears to have a scale length consistent with that of the thermal Jeans length, suggesting that turbulence was not dominant.

Aims. These two results (derived from N_2H^+ (1–0) observations and measurements of the spatial separations of the protostars) probe different density regimes. Our aim is to determine if there is subsonic or less-turbulent gas (than previously reported) in the Spokes cluster when probing higher densities, which would reconcile both previous observational results. To study denser gas it is necessary to carry out observations using transitions with a higher critical density to directly measure its kinematics.

Methods. We present APEX N_2H^+ (3–2) and N_2D^+ (3–2) observations of the NGC2264-D region to measure the linewidths and the deuteration fraction of the higher density gas. The critical densities of the selected transitions are more than an order of magnitude higher than that of N_2H^+ (1–0).

Results. We find that the N_2H^+ (3–2) and N_2D^+ (3–2) emission present significantly narrower linewidths than the emission from N_2H^+ (1–0) for most cores. In two of the spectra, the non-thermal component is close (within $1-\sigma$) to the sound speed. In addition, we find that the three spatially segregated cores, for which no protostar had been confirmed show the highest levels of deuteration.

Conclusions. These results show that the higher density gas, probed with N_2H^+ and N_2D^+ (3–2), reveals more quiescent gas in the Spokes cluster than previously reported. More high-angular resolution interferometric observations using high-density tracers are needed to truly assess the kinematics and substructure within NGC2264-D.

Key words. ISM: clouds – stars: formation – ISM: molecules – ISM: individual (NGC2264-D)

1. Introduction

The current paradigm of cluster formation starts with a highly turbulent cloud, in which dense clumps¹ are close to virial equilibrium (e.g., McKee & Ostriker, 2007; Bate, 2009). This turbulence will decay in a free-fall time if there is no driving mechanism. Theoretical studies show that protostellar outflows might be one mechanism capable to drive turbulence in the cloud (e.g. Li & Nakamura, 2006), which agrees with some observational results (Palau et al., 2007; Fontani et al., 2012). However, other studies have shown that outflows might not have enough energy and momentum to sustain turbulence (Arce et al., 2010), while shells driven by young stars might (Arce et al., 2011).

NGC 2264, located ~ 800 pc away (between 750–913 pc, Dahm & Simon, 2005; Baxter et al., 2009; Naylor & Mayne, 2010), is a well-studied cluster in which we can study the role of turbulence in star formation. Within this cluster there is a rich grouping of protostars, known as NGC 2264 D or as the Spokes cluster (we use both nomenclatures interchangeably in this paper). This region has been observed at (sub)millimeter wavelengths with JCMT/SCUBA and IRAM/30m, where several dense cores were identified (Ward-Thompson et al., 2000; Williams & Garland, 2002; Wolf-Chase et al., 2003; Peretto et al., 2006). *Spitzer* observations of the region revealed an agglomeration of deeply embedded protostars (Class 0/I sources) identified primarily at $24\mu\text{m}$. Teixeira et al. (2006), using a nearest-neighbor analysis, found that these protostars have a characteristic projected spacing, $20\pm 5''$, which is consistent with the thermal Jeans length of the region, $27''$ or 0.104 pc at the distance of 800 pc (calculated using the mean filament density of $3\times 10^4\text{ cm}^{-3}$ from Williams & Garland (2002), and temperature of 17 K from Ward-Thompson et al. (2000)). Since the protostars are embedded in dense material, and the virial mass of the system is lower than the total gas and dust mass (Williams

[★] This publication is based on data acquired with the Atacama Pathfinder Experiment (APEX) under programme 088.F-9322A. APEX is a collaboration between the Max-Planck-Institut für Radioastronomie, the European Southern Observatory, and the Onsala Space Observatory.

¹ Regions that may contain substructure and where several stars might form.

& Garland, 2002; Wolf-Chase et al., 2003; Peretto et al., 2006), the protostars are bound to the filaments and are very likely still tracing the primordial substructure of the cluster. The measured regular spacing (consistent with the thermal Jeans length) of the protostars is thus interpreted as a fossil signature of thermal fragmentation of the parental filament (Teixeira et al., 2006).

Peretto et al. (2006) also observed the 15 cores in the Spokes cluster using dust continuum emission. These dense cores present a mean H_2 density ranging between 10^5 and 10^6 cm^{-3} , and masses of 1.8 to $17.3 M_\odot$ (Wolf-Chase et al., 2003; Peretto et al., 2006). Direct comparison with the *Spitzer* $24 \mu\text{m}$ image shows that the cores identified by Peretto et al. (2006) have $24 \mu\text{m}$ *Spitzer* counterparts (i.e., they harbor protostars) except for DMM-8 and DMM-11. Peretto et al. (2006) also observed these 15 dense cores in N_2H^+ (1–0), which traces high-density gas ($2 \times 10^5 \text{ cm}^{-3}$), and found only lines with supersonic velocity dispersions (Mach ~ 3), which is at odds with the interpretation of thermal Jeans fragmentation. Follow-up observations by Teixeira et al. (2007) using the Submillimeter Array (Ho et al., 2004) of one of the cores, DMM-1, showed that it had fragmented into seven compact 1.3 mm sources, of masses ranging between $0.4 M_\odot$ and $1.2 M_\odot$. The mean separation of these sources within DMM-1 is consistent with the thermal Jeans length of the core, which indicates that the core underwent thermal fragmentation.

The apparent disagreement between the observation of supersonic turbulence in the dense gas and the thermal fragmentation, suggested by the spatial separation of the young stellar objects (YSOs), can be tested. If thermal fragmentation indeed took place in the star formation process in this cluster, low levels of turbulence should still be seen using a higher-density tracer. The Spokes cluster contains high-density gas over an extended region, which could explain the N_2H^+ (1–0) observations by Peretto et al. (2006), which show supersonic turbulence in a dense gas tracer. These observations might not be tracing the densest gas in the star-forming cores, but instead it traces the dense environment containing the entire region. This interpretation can be readily tested with new observations using an even higher-density tracer at similar angular resolutions: N_2H^+ (3–2) or N_2D^+ (3–2). Moreover, the $[N_2D^+/N_2H^+]$ abundance ratio is enhanced in the densest and coldest regions of cores (Caselli, 2002), and it decreased after the protostar was formed (Emprechtinger et al., 2009). Therefore, the N_2D^+ (3–2) observations trace more pristine conditions than N_2H^+ (3–2).

A decrease in the velocity dispersion is expected when going to higher-density tracers, as shown by Myers (1983), Goodman et al. (1998), and Fuller & Myers (1992) in regions with lower average densities. Moreover, Pineda et al. (2010) recently presented observations of dense gas as traced by NH_3 (1,1) where a sharp transition from supersonic to subsonic turbulence is seen in the velocity dispersion. This result suggests that to form low-mass stars, the turbulence needs to be dissipated before the star can be formed. It is possible that in more massive and denser environments this transition would occur at higher densities, and therefore higher-density tracers need to be used. Foster et al. (2009) showed, from their observations of the dense cores in the Perseus molecular cloud, that the cores have subsonic NH_3 (1,1) linewidths regardless of their stellar content or cluster environment. Moreover, even though the effect of the molecular outflows is important in the dynamics of the low-density gas, the dense gas is only locally affected (Pineda et al., 2010, 2013, 2011).

Therefore, by observing the Spokes cluster in a denser-gas tracer than N_2H^+ (1–0), we can determine whether the emission

arising from denser regions is less turbulent. This could provide a test of the thermal-fragmentation hypothesis of the quiescent gas.

2. Data

The observations of N_2H^+ and N_2D^+ (3–2) molecular lines were carried out on 5 September and 4, 8–9, and 11–13 November 2011 with APEX. Every dense core in the Spokes cluster identified by Peretto et al. (2006) that presented a good detection of the N_2H^+ (1–0) line (14 cores) was observed in N_2H^+ (3–2) using the APEX-2 receiver of the Swedish Heterodyne Facility Instrument (SHeFI; Vassilev et al., 2008). The cores with the narrowest N_2H^+ (1–0) lines (eight cores) were also observed in N_2D^+ (3–2) using the APEX-1 receiver of the SHeFI (Vassilev et al., 2008).

Figure 1 shows a JCMT/SCUBA $450 \mu\text{m}$ map of the Spokes cluster, including the locations of the previously identified protostars and our APEX observations. A summary of the sources is listed in Table 1. The observed transitions, their spectroscopic properties, and observational parameters are listed in Table 2. We use the following nomenclature for source identification: MM??, where “??” is the source number (e.g., source D-MM1 of Peretto et al. (2006) is referred to as MM01 hereafter).

The observations used position-switching, with the off-position at $(\alpha_{J2000}=06^{\text{h}}40^{\text{m}}52.57^{\text{s}}, \delta_{J2000}=09^{\circ}32'36.5'')$. They were calibrated by regularly measuring the sky brightness and cold/hot loads in the cabin. All observations used the eXtended bandwidth Fast Fourier Transform Spectrometer (XFFTS), which provides two 2.5 GHz units, with 32,768 channels each unit and 1 GHz overlap. This configuration provides an spectral resolution of 0.082 km s^{-1} and 0.099 km s^{-1} for N_2H^+ and N_2D^+ (3–2), respectively.

All spectra were reduced using CLASS90². Each spectrum had a first- or second-order polynomial fitted to remove the baseline before averaging all scans.

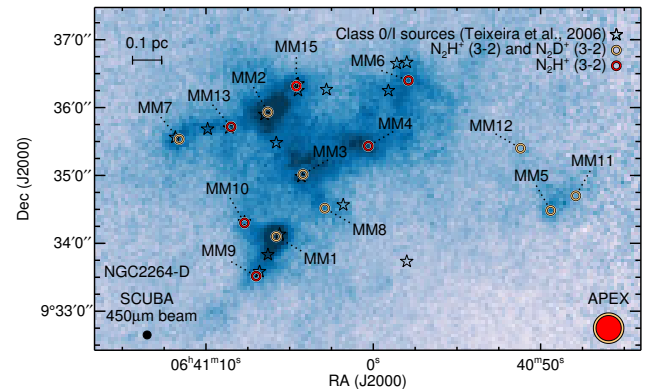


Fig. 1. SCUBA $450 \mu\text{m}$ dust-continuum map for the Spokes cluster (Wolf-Chase et al., 2003). The observed dense cores identified in Peretto et al. (2006) are shown by the circles at their centers (color-coded according to which molecular line tracers were used in their observation). For comparison, the APEX beams corresponding to our observations are also shown in the lower right corner (following the same color-code convention).

² <http://www.iram.fr/IRAMFR/GILDAS>

3. Results

We detected N_2H^+ (3–2) and N_2D^+ (3–2) emission toward all 14 and 8 observed cores respectively. The N_2H^+ (3–2) and N_2D^+ (3–2) spectra are shown in Figures 2 and 3, respectively. In addition, we overplot on these figures the best-fit profiles to the lines.

The N_2H^+ and N_2D^+ (3–2) lines were fitted in IDL³ using a forward-fitting model that takes into account all hyperfine components, with the minimization performed using the `mpfitfun` program (Markwardt, 2009). For a given centroid velocity (v_{LSR}), velocity dispersion (σ_v), and total optical depth (τ_{main}) we computed the optical depth at each velocity as

$$\tau = \tau_{main} \sum_i w_i \exp \left[- (v - v_i - v_{LSR})^2 / (2\sigma_v^2) \right], \quad (1)$$

where w_i and v_i are the relative weight and offset velocity for each hyperfine component. The model spectrum is then generated as

$$T_{MB} = \eta_f [J(T_{ex}) - J(T_{bg})] [1 - e^{-\tau}] \quad (2)$$

where T_{MB} is the main-beam temperature, η_f is the filling fraction of the emission in the beam, T_{ex} is the excitation temperature, T_{bg} is the background brightness temperature (2.73 K), and

$$J(T) = \frac{hv}{k} \frac{1}{\exp(hv/kT) - 1}.$$

Since the extent of the emission is unknown and it is unclear if it is more or less extended than the continuum emission, we assumed a filling fraction of unity, $\eta_f = 1$. Therefore, T_{ex} is obtained from the fit when τ_{main} is well constrained. We also compared the results of fitting the spectra using the HFS mode within CLASS90, where we obtained the same results within the fitted parameter uncertainties. This procedure usually returns well-constrained parameters, but when the total optical depth is poorly constrained ($\tau < 3\sigma_\tau$), we kept the excitation temperature as a fixed parameter. For the N_2H^+ (3–2) line, the excitation temperature was set to the average value obtained from all other spectra, i.e., 6.7 K, because this average excitation temperature provides the typical excitation conditions in the region. For N_2D^+ (3–2), the fit is only poorly constrained and therefore the excitation temperature was set to the value obtained from the N_2H^+ (3–2) fit, because both transitions are optically thin and have similar critical densities. This procedure is similar to that followed in Crapsi et al. (2005).

For most of the cores the fits are good, but there are two cores (MM03 and MM13) that present two distinct components along the line-of-sight. In this case two independent lines were fitted simultaneously, and each of the two components was labeled “a” or “b”. There are two other cores, MM08 and MM04, which show a clear asymmetry in the line profile that suggestive of an additional component along their line-of-sight. Unfortunately, we were unable to separate the blended components. Table 3 shows the results of the hyperfine fitting procedure to the N_2H^+ (3–2) and N_2D^+ (3–2) lines of all sources.

The column densities were calculated using the constant excitation temperature approximation and that the beam filling factor is 1 for both lines, see equations (A.1) and (A.2) from Appendix A, which are based on Caselli et al. (2002).

Figure 4 compares the velocity dispersions obtained from the different molecular lines that we observed and the N_2H^+ (1–0) velocity dispersions reported in Peretto et al. (2006). The velocity dispersion, σ_v , has a thermal, σ_T , and a nonthermal, σ_{NT} ,

Table 4. Column densities

Source	$N(N_2H^+)$ (10^{12}cm^{-2})	$N(N_2D^+)$ (10^{11}cm^{-2})	$N(N_2D^+)/N(N_2H^+)$
MM01	58±1	4.4±0.3	0.0076±0.0006
MM02	56±4	11.2±0.5	0.020±0.002
MM03 [†]	19.5±0.3	12.7±0.7	0.065±0.004
MM04	45±6
MM05	86±14	65±3	0.08±0.01
MM06	41±3
MM07	31±1	2.7±0.4	0.009±0.002
MM08	46±5	2.0±0.9	0.004±0.002
MM09	42±2
MM10	45±3
MM11	0.9±0.1	4.6±0.7	0.5±0.1
MM12	3.0±0.1	3.2±0.5	0.11±0.02
MM13 [†]	10.4±0.2
MM15	60±15

Notes. ^(†) The spectra of sources NGC2264D-MM03 and -MM13 show two components, but since the optically thin model had to be used for at least one of the components, we used the optically thin column density estimate.

component and is given as $\sigma_v = \sqrt{\sigma_T^2 + \sigma_{NT}^2}$. Each panel also indicates, for comparison purposes, expected velocity dispersions whose nonthermal components are $\sigma_{NT} = c_s(10 \text{ K})$ (dashed lines) and $\sigma_{NT} = 2 c_s(10 \text{ K})$ (dotted lines). Figure 4-a shows the comparison of the velocity dispersion obtained from the two different transitions N_2H^+ (1–0) and (3–2); the plot clearly shows *that there is a trend for the velocity dispersion to be narrower for the higher-J transition*. Figure 4-b shows the comparison of the velocity dispersions of the N_2H^+ and N_2D^+ (3–2) molecular lines. From this plot we see that the velocity dispersions of these two high-density tracers agree well.

4. Discussion and conclusion

As stated in section § 1, we aimed to test whether the previous N_2H^+ (1–0) observations of the Spokes cluster were in fact probing the larger extended emission and not the densest gas in the star-forming cores. If this scenario is correct, we would expect the linewidths of higher-J transition emission, tracing higher-density gas, to be narrower. The results presented in the previous section indicate that the denser gas does indeed present narrower linewidths. For N_2H^+ (1–0) lines, as previously discussed in Peretto et al. (2006), the nonthermal velocity dispersions are supersonic and in most of them the $\sigma_{NT} > 2 c_s(10 \text{ K})$. However, in the higher-density gas, traced by N_2H^+ (3–2), the nonthermal velocity dispersion is lower than that of N_2H^+ (1–0). In fact, the N_2H^+ (3–2) velocity dispersions are $\approx 70\%$ of the value derived from N_2H^+ (1–0), and more than half of the total sample shows $\sigma_{NT} \leq 2 c_s(10 \text{ K})$. There are, however, three outlier data points where the velocity dispersion derived from N_2H^+ (3–2) is higher than those from N_2H^+ (1–0). Close inspection reveals that a) one of these outliers corresponds to a poorly constrained second component (MM03b), b) another outlier presents asymmetries in the line profile that clearly suggests the presence of a second unresolved component along the line-of-sight (MM08), and finally, c) the remaining outlier data point is obtained from the spectrum with the lowest signal-to-noise ratio with a large associated uncertainty (MM11). Finally, the velocity dispersions obtained with N_2D^+ (3–2) either agree with those obtained with N_2H^+ (3–2) or are lower. It is important to note there are two

³ Interactive Data Language

cores in our sample that show velocity dispersions consistent (within the $1\text{-}\sigma$ uncertainties) with a sonic nonthermal component: MM03a in N_2H^+ (3–2) and MM08 in N_2D^+ (3–2).

These results thus support the thermal-fragmentation scenario presented in Teixeira et al. (2006). Although the nonthermal velocity dispersions here reported are still broad, they are much narrower than those found previously using N_2H^+ (1–0) single-dish observations (Peretto et al., 2006). It also is important to note that these single-dish observations have a coarse angular resolution ($\approx 17\,840\text{ AU} = 0.086\text{ pc}$ at 800 pc), and the substructure or several components along the line-of-sight could increase the observed linewidth. It is clear that more high-angular resolution interferometric observations using high-density tracers are needed to truly assess the kinematics and substructure within NGC2264-D.

Deuteration can be used as a proxy for the chemical evolution of a core (Crapsi et al., 2005; Emprechtinger et al., 2009; Fontani et al., 2011). For prestellar cores, the deuteration fraction increases as these cores evolve, reaching a maximum at the onset of star formation; the deuteration fraction of the core then begins to decrease as the protostar evolves. For this reason, a high-deuteration fraction in a protostellar core is a particular indicator of youth of the protostar, and a high-deuteration fraction of a prestellar core is an indicator that the core may soon collapse to form a protostar. Table 4 shows that there are four cores (MM03, MM05, MM11, and MM12) with a deuteration fraction at least a factor of 3 higher than the rest of the sample, where the largest difference is a factor of 125. Three of these cores are spatially separated from the main cluster (see Figure 1) and are embedded in a less dense region. Furthermore, Table 1 shows that no protostar is identified in MM11, and both MM05 and MM12 have faint $24\text{ }\mu\text{m}$ sources that have no counterparts at other infrared wavelengths, meaning that these two cores could potentially be harboring either very young or very low mass protostars (additional investigation is necessary to confirm the protostellar nature of MM05 and MM12). Our results thus suggest that these three cores are the least evolved in the Spokes cluster, i.e., closest to the very earliest star formation evolutionary phase. Friesen et al. (2010) found similar results in their analysis of the cores in the Ophiuchus B2 region, where the deuteration fraction decreases with proximity to protostellar cores. The spectrum of core MM03, which is located within the dense region of the Spokes cluster, shows two components, as mentioned. Additional investigation, requiring higher angular and spectral resolution data, is needed to understand the deuteration fraction in this particular core. Moreover, we found no correlation between the level of deuteration and velocity dispersion. Although these few data points make this result uncertain, they agree with what was found in Friesen et al. (2013) in a larger study of nearby low-mass cores.

5. Summary

We summarize our main results and conclusions as follows:

1. We observed in the Spokes cluster 14 cores in N_2H^+ (3–2) and 8 cores in N_2D^+ (3–2) with APEX; the measured linewidths are overall narrower than those of previous N_2H^+ (1–0) observations, $\sigma_v[\text{N}_2\text{H}^+(3-2)] \sim 0.7 \sigma_v[\text{N}_2\text{H}^+(1-0)]$.
2. The three cores (MM03b, MM08, and MM11) that do not show narrower N_2H^+ (3–2) linewidths than the N_2H^+ (1–0) linewidths are cores with more than one component along the line-of-sight or low signal-to-noise spectra.

3. The denser gas, probed by higher J-transitions of N_2H^+ and N_2D^+ , presents lower levels of turbulence (nonthermal velocity dispersion) and in two cases approaches the sound speed. These results support the scenario of thermal fragmentation in the expectation that higher-angular resolution observations and/or higher-density tracers would find more quiescent gas.
4. Finally, we find that the three cores of our sample, spatially separated from the main Spokes cluster, are likely the youngest, based on their higher deuteration values.

Acknowledgements. We thank Gary Fuller, Charlie Lada, Paola Caselli, and the anonymous referee for comments that improved the paper. We also thank the staff at the APEX telescope for performing the observations presented in this paper in service-mode. JEP has received funding from the European Community's Seventh Framework Programme (FP7/2007–2013/) under grant agreement No 229517. This publication is supported by the Austrian Science Fund (FWF).

References

- Arce, H. G., Borkin, M. A., Goodman, A. A., Pineda, J. E., & Beaumont, C. N. 2011, *ApJ*, 742, 105
- Arce, H. G., Borkin, M. A., Goodman, A. A., Pineda, J. E., & Halle, M. W. 2010, *ApJ*, 715, 1170
- Bate, M. R. 2009, *MNRAS*, 392, 590
- Baxter, E. J., Covey, K. R., Muench, A. A., et al. 2009, *AJ*, 138, 963
- Caselli, P. 2002, *Planet. Space Sci.*, 50, 1133
- Caselli, P., Walmsley, C. M., Zucconi, A., et al. 2002, *ApJ*, 565, 344
- Crapsi, A., Caselli, P., Walmsley, C. M., et al. 2005, *ApJ*, 619, 379
- Dahm, S. E. & Simon, T. 2005, *AJ*, 129, 829
- Emprechtinger, M., Caselli, P., Volgenau, N. H., Stutzki, J., & Wiedner, M. C. 2009, *A&A*, 493, 89
- Fontani, F., Palau, A., Busquet, G., et al. 2012, *MNRAS*, 423, 1691
- Fontani, F., Palau, A., Caselli, P., et al. 2011, *A&A*, 529, L7+
- Foster, J. B., Rosolowsky, E. W., Kauffmann, J., et al. 2009, *ApJ*, 696, 298
- Friesen, R. K., Di Francesco, J., Myers, P. C., et al. 2010, *ApJ*, 718, 666
- Friesen, R. K., Kirk, H. M., & Shirley, Y. L. 2013, *ApJ*, 765, 59
- Fuller, G. A. & Myers, P. C. 1992, *ApJ*, 384, 523
- Goodman, A. A., Barranco, J. A., Wilner, D. J., & Heyer, M. H. 1998, *ApJ*, 504, 223
- Ho, P. T. P., Moran, J. M., & Lo, K. Y. 2004, *ApJ*, 616, L1
- Li, Z.-Y. & Nakamura, F. 2006, *ApJ*, 640, L187
- Markwardt, C. B. 2009, in *Astronomical Society of the Pacific Conference Series*, Vol. 411, *Astronomical Data Analysis Software and Systems XVIII*, ed. D. A. Bohlender, D. Durand, & P. Dowler, 251–+
- McKee, C. F. & Ostriker, E. C. 2007, *ARA&A*, 45, 565
- Myers, P. C. 1983, *ApJ*, 270, 105
- Naylor, T. & Mayne, N. J. 2010, *Highlights of Astronomy*, 15, 763
- Palau, A., Estalella, R., Ho, P. T. P., Beuther, H., & Beltrán, M. T. 2007, *A&A*, 474, 911
- Peretto, N., André, P., & Belloche, A. 2006, *A&A*, 445, 979
- Pineda, J. E., Goodman, A. A., Arce, H. G., et al. 2010, *ApJ*, 712, L116
- Pineda, J. E., Goodman, A. A., Arce, H. G., et al. 2013, In prep.
- Pineda, J. E., Goodman, A. A., Arce, H. G., et al. 2011, *ApJ*, 739, L2+
- Teixeira, P. S., Lada, C. J., Young, E. T., et al. 2006, *ApJ*, 636, L45
- Teixeira, P. S., Zapata, L. A., & Lada, C. J. 2007, *ApJ*, 667, L179
- Vassilev, V., Meledin, D., Lapkin, I., et al. 2008, *A&A*, 490, 1157
- Ward-Thompson, D., Zylka, R., Mezger, P. G., & Sievers, A. W. 2000, *A&A*, 355, 1122
- Williams, J. P. & Garland, C. A. 2002, *ApJ*, 568, 259
- Wolf-Chase, G., Moriarty-Schieven, G., Fich, M., & Barsony, M. 2003, *MNRAS*, 344, 809

Table 1. List of observed sources

Source	R.A. (hh:mm:ss)	Decl. (dd:mm:ss)	σ_v^a (km s ⁻¹)	On-source time		# YSOs within APEX beams ^b
				N ₂ H ⁺ (3–2) (min)	N ₂ D ⁺ (3–2) (min)	
MM01	06:41:05.8	+09:34:06	0.59	4.0	23.0	1 (7) ^c
MM02	06:41:06.3	+09:35:56	0.51	2.3	28.0	1
MM03	06:41:04.2	+09:35:01	0.26	3.3	24.0	1
MM04	06:41:00.3	+09:35:26	0.81	3.3	...	0 (1) ^d
MM05	06:40:49.4	+09:34:29	0.42	13.4	24.0	0 (1) ^d
MM06	06:40:57.9	+09:36:24	0.55	3.3	...	0 (1) ^d
MM07	06:41:11.6	+09:35:32	0.59	3.3	17.0	1
MM08	06:41:02.9	+09:34:31	0.34	3.3	31.0	0
MM09	06:41:07.0	+09:33:31	0.55	3.3	...	1
MM10	06:41:07.7	+09:34:18	0.72	3.3	...	1
MM11	06:40:47.9	+09:34:42	0.30	13.7	33.0	0
MM12	06:40:51.2	+09:35:24	0.38	8.0	79.0	0 (1) ^d
MM13	06:41:08.5	+09:35:43	0.89	6.3	...	1
MM15	06:41:04.6	+09:36:19	0.64	13.7	...	2

Notes. ^(a) Velocity dispersion from Peretto et al. (2006) derived using N₂H⁺ (1–0) fits.

^(b) Number of protostars located within the APEX HPBW (see Table 2) (Peretto et al., 2006, and references therein), (Teixeira et al., 2006).

^(c) Targeted SMA observations of this core revealed additional compact millimeter sources undetected in the infrared (Teixeira et al., 2007).

^(d) The value in parenthesis corresponds to the number of faint 24 μm sources that have no other wavelength counterpart (and therefore we cannot confirm their protostellar nature).

Table 2. Observed transitions and observational parameters

Transition	Frequency (GHz)	HPBW (")	channel spacing (kHz)	η _{MB}	B (MHz)	μ (D)
N ₂ D ⁺ (3–2)	231.3219119	27.0	76.29	0.0989	0.75	38554.719
N ₂ H ⁺ (3–2)	279.511862	22.3	76.29	0.0818	0.74	46586.867

Notes. η_{MB} is the main-beam efficiency of the APEX telescope, B is the rotational constant of the molecule, and μ is the dipole moment of the molecule.

Table 3. Best-fit line parameters for sources in NGC2264-D

Source ^a	N ₂ H ⁺ (3–2)					N ₂ D ⁺ (3–2)			
	T _{ex} (K)	V _{LSR} (km s ⁻¹)	σ _v (km s ⁻¹)	τ _{main}	W (K km s ⁻¹)	V _{LSR} (km s ⁻¹)	σ _v (km s ⁻¹)	τ _{main}	W (K km s ⁻¹)
MM01	10.90±0.03	6.405±0.004	0.495±0.003	8.0±0.2	16.07±0.08	6.26±0.02	0.38±0.02	<0.07	0.43±0.03
MM02	7.37±0.05	5.713±0.009	0.339±0.007	10.5±0.6	5.9±0.1	5.75±0.02	0.43±0.02	<0.19	0.57±0.02
MM03a	5.6±0.2	7.15±0.02	0.22±0.03	4±1	5.89±0.09	7.11±0.03	0.28±0.03	<0.27	0.52±0.03
MM03b	6.7	6.25±0.05	1.33±0.04	<0.90	...	5.65±0.05	0.54±0.06	<0.11	...
MM04	6.34±0.07	4.75±0.02	0.61±0.02	4.2±0.5	4.8±0.1
MM05	4.25±0.03	4.72±0.02	0.33±0.02	8±1	1.04±0.04	4.79±0.02	0.36±0.02	<1.04	0.50±0.03
MM06	6.58±0.03	5.694±0.007	0.349±0.007	6.9±0.4	3.96±0.06
MM07	8.53±0.03	3.366±0.005	0.452±0.005	4.7±0.2	7.53±0.06	3.72±0.07	0.47±0.07	<0.04	0.19±0.03
MM08	6.17±0.05	6.75±0.01	0.65±0.02	3.9±0.4	4.59±0.06	5.97±0.06	0.23±0.07	<0.06	0.07±0.03
MM09	7.74±0.03	6.103±0.006	0.436±0.005	6.4±0.2	6.76±0.06
MM10	6.32±0.04	6.66±0.01	0.51±0.01	5.0±0.4	4.38±0.06
MM11	6.7	4.72±0.05	0.50±0.05	<0.11	0.27±0.03	4.78±0.05	0.43±0.06	<0.07	0.19±0.03
MM12	6.7	5.31±0.02	0.39±0.02	<0.52	0.89±0.04	5.38±0.05	0.36±0.05	<0.06	0.13±0.02
MM13a	6.7	4.20±0.02	0.42±0.02	<1.20	3.14±0.07
MM13b	6.7	5.84±0.03	0.49±0.03	<0.61
MM15	4.18±0.05	5.85±0.02	0.38±0.03	5±1	0.89±0.05

Notes. ^(a) If the spectrum shows two components, they were both fitted, listed in different rows, and labeled as components a and b.

^(b) We were unable to derive W for each of the two components – the value listed for component a corresponds to the integrated W for both components.

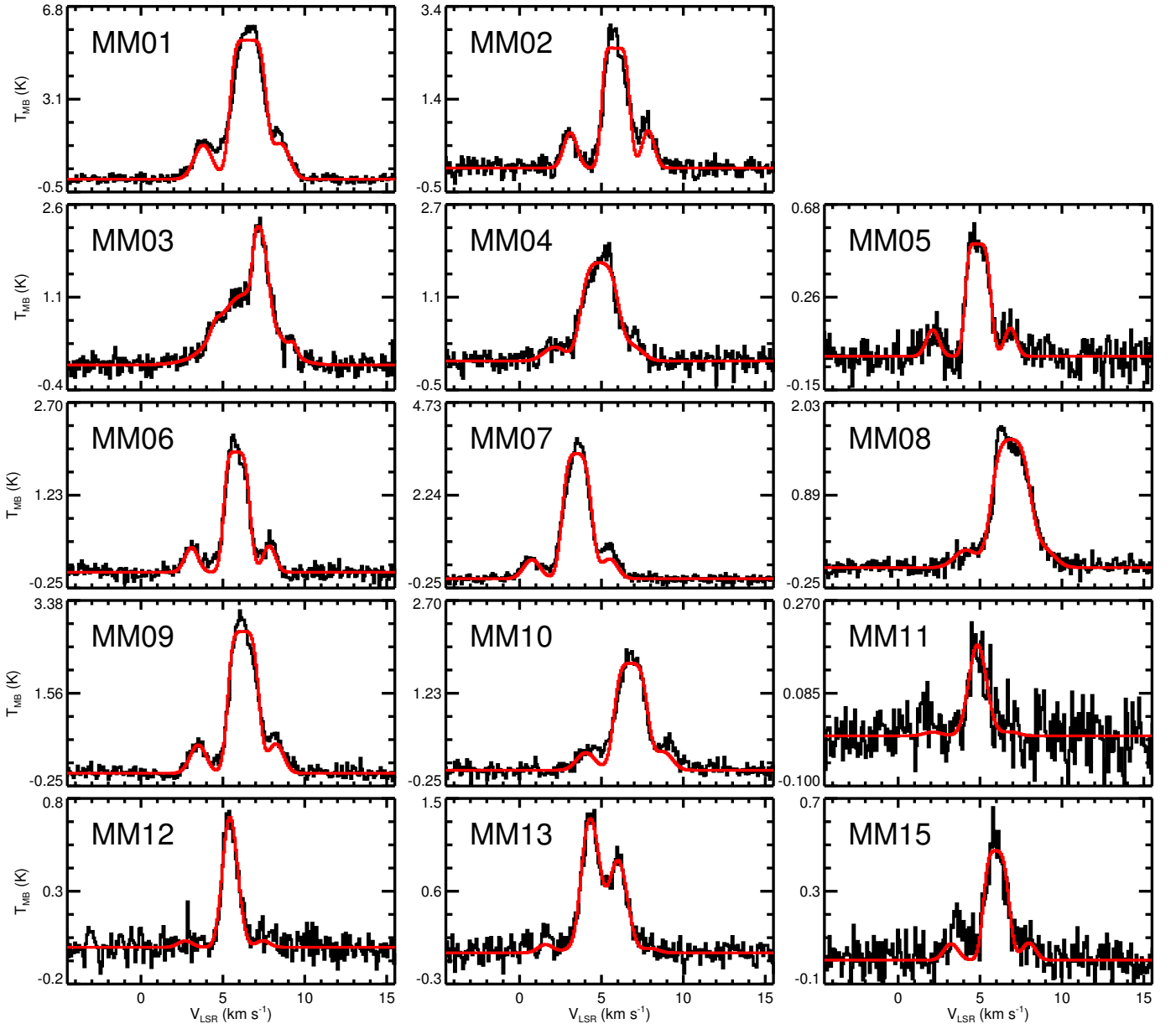


Fig. 2. Observed N_2H^+ (3–2) spectra toward the sources. The red curve is the best-fit model to the observations, whose fit parameters are shown in Table 3.

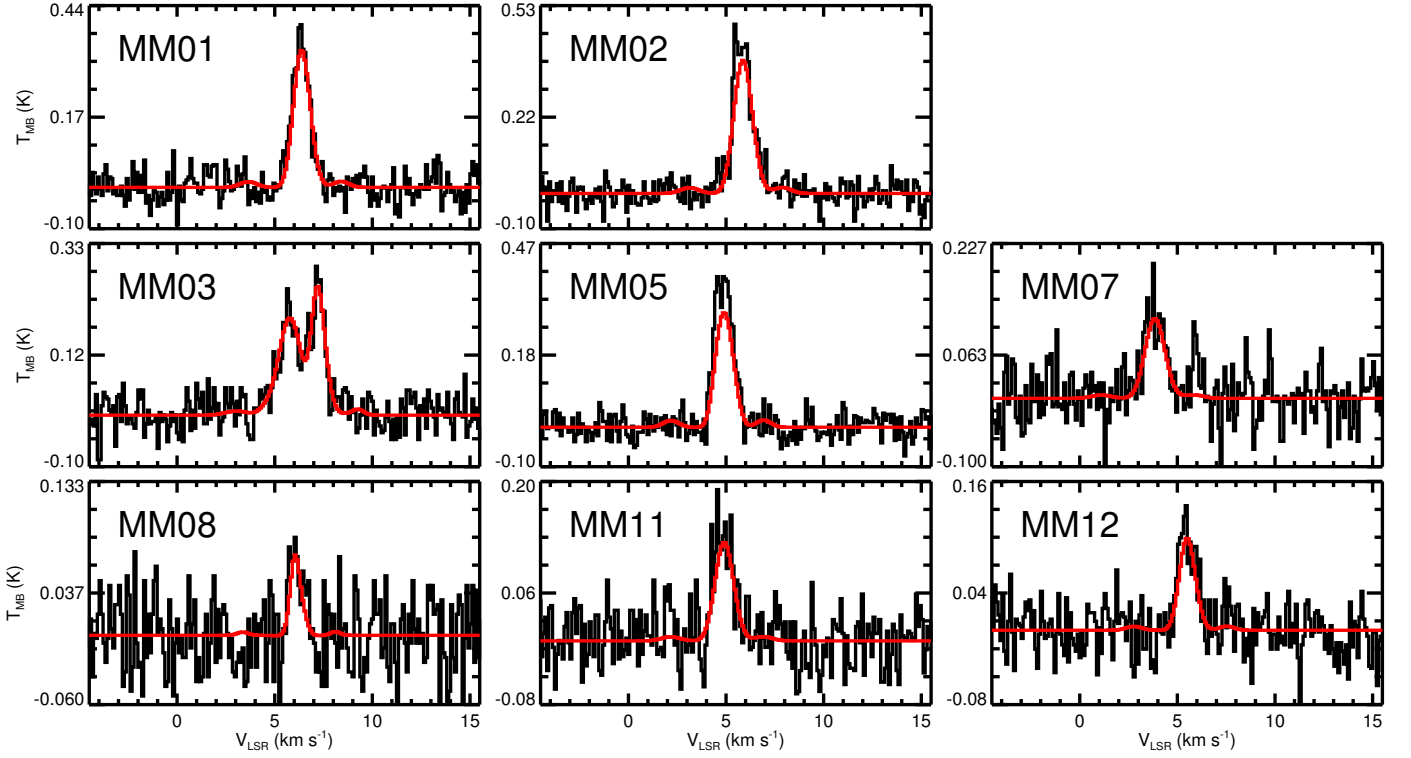


Fig. 3. Observed N_2D^+ (3–2) spectra toward the sources. The red curve is the best-fit model to the observations, whose fit parameters are shown in Table 3.

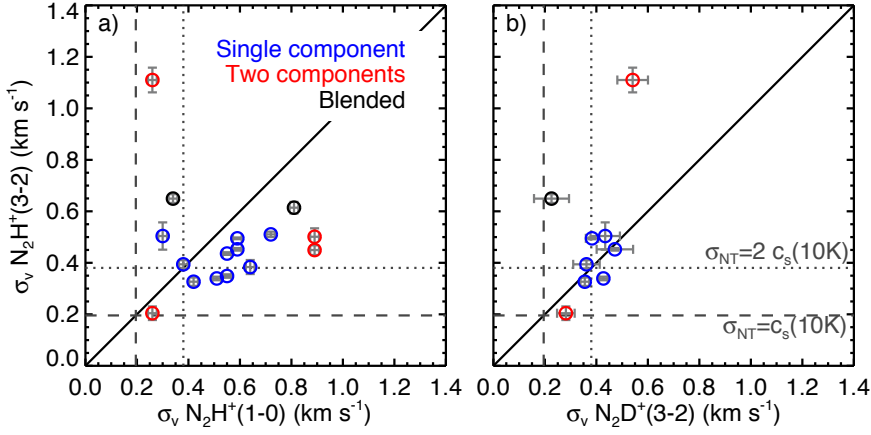


Fig. 4. Comparison of the velocity dispersion of different molecular lines. Cores listed as showing two components (see Table 3) are shown as red symbols, cores that appear to have blended components are shown in black, and the rest are shown as blue symbols. Dashed and dotted lines show the expected velocity dispersion for the cases where the nonthermal velocity dispersion, σ_{NT} , equals $c_s(10\text{ K})$ or $2c_s(10\text{ K})$, where $c_s(10\text{ K})$ is the sound speed of the average molecule at 10 K (for a mean molecular weight of $\mu_m = 2.33$).

Appendix A: Column density determination

The column density is calculated for the optically thick and thin cases using different expressions, but in both cases assuming a beam filling factor of 1. In the optically thick case,

$$N_{Tot} = 2.01 \times 10^{13} \left(\frac{\sigma_v}{\text{km s}^{-1}} \right) \left(\frac{\mu}{\text{Debye}} \right)^{-2} \frac{1}{(J+1)} \frac{\tau}{(1 - e^{-T_0/T_{ex}})} \frac{Q_{rot}(T)}{e^{-J(J+1)hB/kT_{ex}}}, \quad (\text{A.1})$$

and in the optically thin case,

$$N_{Tot} = 8.01 \times 10^{12} \left(\frac{W}{\text{K km s}^{-1}} \right) \left(\frac{\mu}{\text{Debye}} \right)^{-2} \frac{1}{(J+1)} \left[\frac{1 \text{ K}}{J_v(T_{ex}) - J_v(T_{bg})} \right] \frac{1}{(1 - e^{-T_0/T_{ex}})} \frac{Q_{rot}(T)}{e^{-J(J+1)hB/kT_{ex}}}, \quad (\text{A.2})$$

which are the same as eqs. (A1) and (A4) in Caselli et al. (2002) after rearranging terms and using that

$$A_{J+1 \rightarrow J} = \frac{64\pi^4}{3hc} \nu^3 |\mu_{J+1 \rightarrow J}|^2 = 1.164 \times 10^{-11} \left(\frac{\nu}{\text{GHz}} \right)^3 \left(\frac{\mu}{\text{Debye}} \right)^2 \left(\frac{J+1}{2J+3} \right) \text{ s}^{-1} \quad (\text{A.3})$$

$$|\mu_{J+1 \rightarrow J}|^2 = \mu^2 \frac{J+1}{2J+3} \quad (\text{A.4})$$

$$g_J = 2J+1 \quad (\text{A.5})$$

$$E_J = J(J+1)hB \quad (\text{A.6})$$

$$Q_{rot}(T) = \sum_{J=0}^{\infty} (2J+1) e^{-J(J+1)hB/kT}, \quad (\text{A.7})$$

where $T_0 \equiv h\nu/k$ and $J_v(T) = T_0/[\exp(T_0/T) - 1]$. The partition function is calculated using the first 100 levels.